Macromolecular Research, Vol. 22, No. 9, pp 1032-1041 (2014)
DOI 10.1007/s13233-014-2140-8

www.springer.com/13233
pISSN 1598-5032 eISSN 2092-7673

Effect of Magnesium Hydroxide Nanoparticles with Rod and Plate Shape on Mechanical and Biological Properties of Poly(*L*-lactide) Composites

Chang Hun Kum[1,3], Seong Ho Seo[1], Sung Nam Kang[1,2], Bang Ju Park[4], Dong June Ahn[3], Yoon Ki Joung*[,1,2], and Dong Keun Han*[,1,2]

[1]*Center for Biomaterials, Biomedical Research Institute, Korea Institute of Science and Technology, Seoul 136-791, Korea*
[2]*Department of Biomedical Engineering, Korea University of Science and Technology, Daejeon 305-350, Korea*
[3]*Department of Chemical and Biological Engineering, Korea University, Seoul 136-701, Korea*
[4]*Department of Electronic Engineering and Institute of Gachon Fusion Technology, Gachon University, Gyeonggi 461-701, Korea*

Received May 19, 2014; Revised June 3, 2014; Accepted June 9, 2014

Abstract: Two kinds of magnesium hydroxide ($Mg(OH)_2$) rods (Mg-Rod, 150 and 350 nm in size) and plates (Mg-PL, 60 and 300 nm) were prepared, and blended with poly(*L*-lactide) (PLLA) to obtain PLLA/$Mg(OH)_2$ composites to investigate the effect of the shape and size of $Mg(OH)_2$ particles. The structure, morphology, pH change, thermal and mechanical properties, cytotoxicity, and inflammation of $Mg(OH)_2$ control and PLLA/$Mg(OH)_2$ composites were evaluated. PLLA/Mg-Rod150 (30%) composite showed a 50% higher tensile strength and a 45% improved modulus as compared with PLLA/Mg-PL300 30% composite. Although Mg-Rods displayed similar cell viability (above 80%) as compared to Mg-PLs, the expression levels of TNF-α from Mg-PL60 gradually increased with increasing concentrations from 1 to 300 μg. This indicates that Mg-PL60 had a potential cytotoxicity due to endocytosis. In addition, the byproduct of PLLA/Mg-Rods composite was more effectively neutralized than that of the PLLA/Mg-PLs composite, but cell viability and the expression levels of TNF-α were similar. Therefore, the use of our PLLA/Mg-Rod composite system would be a promising strategy to prevent the current fatal problems in biomedical applications including biodegradable implants such as stents.

Keywords: poly(*L*-lactide), magnesium hydroxide, shape, mechanical property, inflammation.

Introduction

Poly(*L*-lactide) (PLLA) has the characteristics of being degradable and absorbable in human body, and recently attracted considerable attention as a biomaterial.[1-4] PLLA was degraded by chain hydrolysis and enzymes and was completely absorbed in the human body through the Krebs cycle.[5,6] However, acidic materials are produced during the degradation of PLLA, thereby leading to cytotoxicity and inflammation response.[7-9] Andersson *et al.* verified the inflammation response through a homogeneous hydrolytic chain cleavage mechanism and confirmed to suppress inflammation response by paclitaxel-loaded PLLA microspheres.[10] Kontio *et al.* reported that PLLA resulted in a chronic inflammatory reaction in an *in vivo* experiment.[11]

Many studies have been conducted to prevent cytotoxicity and inflammation response induced during polylactide degradation.[12-14] Vogt *et al.* reported that intravascular restenosis can be prevented by using a polylactide stent containing paclitaxel.[12] Further research is currently being conducted to prevent polylactide inflammation using other drugs such as antitumor agents, which however can cause side effects in the human body.[13,14] In our previous study, we prepared magnesium hydroxide ($Mg(OH)_2$) for neutralizing acidic materials, which are generated during the degradation of polylactide, and the cell cytotoxicity and inflammation response can be effectively suppressed by pH neutralization effect.[15]

However, it is known that the mechanical properties are reduced because of the immiscibility between PLLA and ceramic magnesium hydroxide. Especially, the irregular plate crystal structure of magnesium hydroxide has negative effects on its mechanical properties.[16,17] Many studies have carried out to control the crystal structure of magnesium hydroxide.[18-20] Dehong *et al.* reported that magnesium hydroxide can be grown in the form of rods through a co-precipitation process.[18] Henrist *et al.* stated that different types of magnesium hydroxide can be grown by suitably adjusting the base

*Corresponding Authors. E-mails: dkh@kist.re.kr or ykjoung@kist.re.kr

material (NH_3OH, NaOH, or mixture) and temperature.[19] In particular, Jianping *et al.* showed that the mechanical properties of magnesium hydroxide can be improved by blending $Mg(OH)_2$ nanorods with ethylene-vinyl acetate polymer.[21] These $Mg(OH)_2$ crystalline rods can be more beneficial for the crystal orientation in the polymer than irregular plate crystals.[16] The shape and size of the particle were known to cause the foreign-body giant cell (FBGC) reaction and cell cytotoxicity in the human body.[10,22] The FBGC reaction depends on five factors of the particle: gross size, tissue quantity per unit volume, shape, surface topography, and hydrophobicity/hydrophilicity of the particle surface. Wen e*t al.* demonstrated that cytotoxicity (SK-BR-3 cell) occurred for gold nanoparticles (2-100 nm) of 40 and 70 nm sizes because of endocytosis, but was not generated for sizes below 10 and above 80 nm.[23]

In this study, $Mg(OH)_2$ rods (Mg-Rod, 150 and 350 nm in size) and $Mg(OH)_2$ plates (Mg-PL, 60 and 300 nm) were prepared, and each sample was blended with PLLA. The structures of the obtained $Mg(OH)_2$ was examined using Fourier transform infrared (FTIR) spectroscopy, X-ray diffraction (XRD), and field emission scanning electron microscopy (FE-SEM). The thermal properties and mechanical properties as well as inflammation response of the PLLA/$Mg(OH)_2$ composites were evaluated.

Experimental

Materials. Magnesium sulfate ($MgSO_4$), sodium hydroxide (NaOH), and ethylene diamine were purchased from Sigma-Aldrich (USA). *L*-Lactide was purchased from Boehringer (Germany), recrystallized from ethyl acetate, and stored under a N_2 atmosphere at -5 ºC. Stannous octoate was purchased from Sigma (USA) and was used as 1% distilled toluene solution. Chloroform was used to dry the samples by refluxing over CaH_2. U-937 cell (human monocyte) was purchased from the Korean cell line bank (Korea) and the endothelial growth medium (EGM)-2 was purchased from Lonza (Switzerland). Roswell park memorial Institute medium (RPMI 164) and a live/dead kit were purchased from Introgen (Japan).

Synthesis of Magnesium Hydroxide. The $Mg(OH)_2$ crystalline rods were prepared *via* the hydrothermal method using $MgSO_4$. $MgSO_4$ (12 g) and 100 mL of ethylene diamine solution (75% in distillated water) were added to a 1-neck round flask (250 mL). The flask was heated up to 175 ºC and was maintained for 18 and 36 h. After cooling to room temperature, the white $Mg(OH)_2$ rods were collected, and washed several times with distilled water and absolute ethanol. The washed product was filtered and dried in a vacuum oven at 60 ºC for 24 h to remove the residual solvent, in which the particles were ultimately produced at a yield of 76.4%. In addition, $Mg(OH)_2$ plates were prepared by a general precipitation method using $MgSO_4$ (12 g) and sodium hydroxide (4 g).[24]

Preparation of PLLA/$Mg(OH)_2$ Composite Films. For the preparation of the solvent-cast films, 2 g of PLLA and 0.2 g of $Mg(OH)_2$ crystals were dissolved in 100 mL of chloroform at room temperature. The mixture was then poured into a Teflon dish, and the solvent was evaporated in air at room temperature for 24 h. The resulting films were dried in vacuum at room temperature for 24 h. The films were removed from the Teflon dish using liquid nitrogen. The thickness of the film was measured with a micrometer and confirmed to be 2 mm.

Characterization of $Mg(OH)_2$ and PLLA/$Mg(OH)_2$ Composites. The $Mg(OH)_2$ crystal was characterized by using FTIR (Spectrum 100, Perkin Elmer, USA) employing a type of potassium bromide pellet. X-Ray diffraction (XRD; D/MAX-2500 Rigaku, Japan) was performed using CuK_α radiation (wavelength: 1.5418 Å) at room temperature. For scanning electron microscopy (SEM; XL30, Philips, Netherlands), each $Mg(OH)_2$ powders were mounted on an aluminum stub, and the surface was coated with platinum with a sputter coater before observation. TGA thermograms of PLLA/$Mg(OH)_2$ composites were recorded at a heating rate of 10 ºC/min from 100 to 800 ºC under a nitrogen atmosphere. Differential scanning calorimetry DSC (DSC; DSC 2010, TA, USA) was carried out with the second run at a heating rate of 10 ºC/min from 50 to 250 ºC under nitrogen atmosphere. The molecular weights of the composites were measured by gel permeation chromatography (GPC; 414 GPC system, Waters, USA), which resulted in the weight-average molecular weight (M_w) of 310,000 and the degraded composite films were also observed using SEM. The pH change over time was measured in order to confirm the acidity of the films, along with the neutralization of lactic acid, using a shaking water bath (BS-20, Jeio Tech, Korea) that was set up at 80 ºC and 100 rpm. The mechanical properties of the film such as tensile strength, elongation, and tensile modulus were measured by a universal testing machine (UTM; Instron 4464, Instron, USA) according to ASTM D638-00. The gauge length was 5 cm, and the crosshead speed was 1 cm/min.

Cell Culture. U-937 cells were cultured in Roswell park memorial institute medium (RPMI) 1640, 10% inactivated fetal bovine serum, 1% penicillin, and streptomycin in 5% CO_2 at 37 ºC. Cells were passaged every 2-3 days. U-937 cells were cultured to about 80% confluence and further incubated in a fresh medium containing the above reagents. The cells to be used were differentiated into macrophages through treatment with 100 nM phorbol 12-myristate 13-acetate (PMA) for 48 h.

Cell Viability Assay by CCK-8 and Live/Dead Cell Staining. The U-937 cell viability was analyzed by CCK-8 (Dojindo Molecular Technology, Inc., Rockville, USA) according to the manufacturer's protocol. The optical density (OD) was measured with a microplate reader (Thermo Scientific, Multiskan, USA) at 450 nm. The U-937 cell was treated with $Mg(OH)_2$ (5% in distillated water) or the degradable byproduct (1.0 mg).

The cell was stained with a live/dead cell staining kit. The treated cell was rinsed with phosphate-buffered saline (PBS) solution and incubated in staining solution at 37 °C for 30 min, followed by washing with PBS solution. The constructs were then visualized by a fluorescent microscope (U-RFL-T(CKX41), Olympus, Japan). Healthy cells showed green fluorescence, while the nuclei of dead cells were stained in red.

Analysis of TNF-α Expression Level. U-937 cells (5×10^4 cells/well) were seeded in the wells of a 24-well culture plate and then were incubated in the presence of EGM-2 medium for 24 h at 37 °C. When each cell was cultured to about 80% confluence, it was treated with $Mg(OH)_2$ (5% in distillated water) or the degradable byproduct (1.0 mg) of the film and incubated for 24 h at 37 °C. The medium was removed to determine TNF-α concentration using enzyme-linked immunosorbent assay (ELISA) method.

Results and Discussion

Synthesis of $Mg(OH)_2$ Nanorods and Plates. The magnesium hydroxide rods (Mg-Rods) and plates (Mg-PLs) were synthesized *via* the hydrothermal and base precipitation methods, respectively.

Figure 1(A) shows the FTIR spectra of Mg-Rod150 (length: 150 nm), Mg-Rod350 (length: 350 nm), Mg-PL60 (diameter: 60 nm), and Mg-PL300 (diameter: 300 nm). The sharp peak at 3693 cm^{-1} indicated -OH stretching vibration in the crystal structure of $Mg(OH)_2$, and was observed for Mg-Rod150, Mg-Rod350, Mg-PL60, and Mg-PL300, irrespective of the shape, indicating that $Mg(OH)_2$ was successfully synthesized.[24,25]

Figure 1(B) shows the XRD patterns of Mg-Rod150, Mg-Rod350, Mg-PL60, and Mg-PL300. All the typical diffraction peaks (2θ; 18.5, 32.6, 50.5, 58.7, 61.9, and 68.2°, respectively) were indexed *via* the hexagonal structure of magnesium hydroxide with lattice constants by comparing with the values in Joint committee on powder diffraction standards (JCPDS) file number 7-239.[18,19,26] The peaks of the XRD pattern mean that a plate shaped $Mg(OH)_2$ possessed a very small size, which can be calculated from the full width at half-maximum (FWHM) of the different diffraction peaks by means of the Debye-Scherrer formula.[29] In particular, the Miller indices along the directions [001], [101], and [110] in the crystalline structure indicate either plate-shaped or rod-shaped morphology. Dimensions of 5.1 nm along [001] and 13.1 nm along [101] demonstrate that the particles had rod-shaped morphology with layers stacked in the [001] direction, while dimensions of 10.9, 14.6, and 12.5 nm along the directions [001], [101], and [110], respectively, signified plate-shaped morphology.[18] The results of crystal size estimation using the Debye-Scherrer equation were given in Table I.[19] The intensity ratio I_{001}/I_{110} (1.81 and 1.76) of the rods exhibited a higher value than that (1.21 and 1.28) of the plate morphology, signifying a more pronounced orientation of the rods towards the incident X-ray radiation.[21,26]

Figure 2 presents the morphology of Mg-Rod150, Mg-Rod350, Mg-PL60, and Mg-PL300 obtained by FE-SEM. While Mg-Rod150 and Mg-Rod350 were produced in the shape of rods, Mg-PL60 and Mg-PL300 were shaped as irregular thin plates. The sizes of the different $Mg(OH)_2$ in the SEM images were measured with the Image-J program. The width and length of the Mg-Rod150 rods were 29±4 and 149±23 nm, whereas those of the Mg-Rod350 rods were 31±3 and 379±74 nm, respectively. Furthermore, the diameters of Mg-PL60 and Mg-PL300 plates were 66±7 and 353±142 nm, respectively. These results were confirmed that $Mg(OH)_2$ was synthesized in the shapes of rods and irregular thin plates.

Thermal and Mechanical Properties of PLLA/$Mg(OH)_2$ Composites. Figure 3(A) displays the TGA thermaograms of PLLA, Mg-Rod150, PLLA/Mg-Rod150 10%, PLLA/Mg-Rod150 20%, and PLLA/Mg-Rod150 30% composites. Since Mg-Rod150 was typically used in this study, it is concluded that the weight loss caused by the dehydration of $Mg(OH)_2$

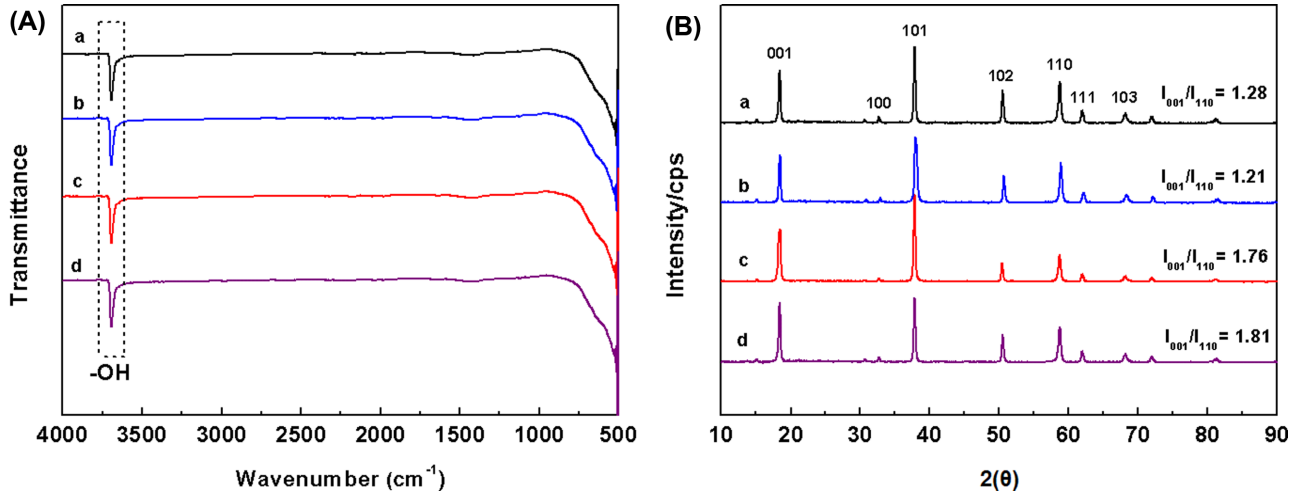

Figure 1. (A) FTIR spectra and (B) XRD patterns of (a) Mg-PL60, (b) Mg-PL300, (c) Mg-Rod150, and (d) Mg-Rod350.

Table I. Crystallite Size from the XRD Patterns of $Mg(OH)_2$ Plate and Rod

Sample	Peak Position *d* Value (nm)	Miller Index (hkl)	Full Width at Half-Maximum (deg)	Crystallite Size[a] (nm)
Mg-PL60	0.4765	001	0.73	10.9
	0.2362	101	0.51	14.6
	0.1568	110	0.56	12.5
Mg-PL300	0.4765	001	0.46	17.3
	0.2362	101	0.40	18.5
	0.1568	110	0.33	21.5
Mg-Rod150	0.4765	001	1.53	5.1
	0.2362	101	0.56	13.1
	0.1568	110	0.32	22.3
Mg-Rod350	0.4765	001	1.17	6.7
	0.2362	101	0.47	15.7
	0.1568	110	0.23	31.3

[a]Crystallite size was estimated by Scherrer equation.

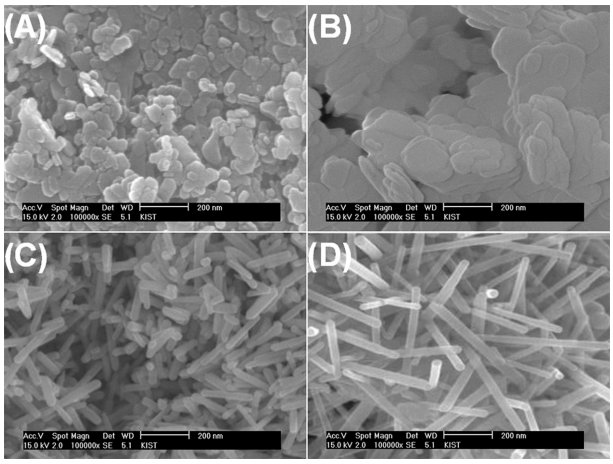

Figure 2. SEM images of (A) Mg-PL60, (B) Mg-PL300, (C) Mg-Rod150, and (D) Mg-Rod350. The magnification of the images is ×100,000.

started at around 400 °C.[27] The observed degradation pattern indicated the weight loss of PLLA at 300 °C.[28]

The thermal decomposition of PLLA/Mg-Rod150 10% composites occurred in two phases, with the first weight loss occurring at approximately 270 °C and the second weight loss at 400 °C. The first weight loss was caused by PLLA decomposition in the PLLA/Mg-Rod150 composites and the second weight loss was caused by dehydration of $Mg(OH)_2$. Moreover, as the content of Mg-Rod150 increased from 10 to 30%, the temperature at the first weight loss increased from 270 to 310 °C, meaning that the strong thermal resistance of $Mg(OH)_2$ contributed to an increase in the degradation temperature of the PLLA. Thermal decomposition of PLLA/Mg-Rod350, PLLA/Mg-PL60, and PLLA/Mg-PL300 composites revealed a similar pattern to that of PLLA/Mg-Rod150 (data not shown).

Figure 3(B) shows the DSC traces of the PLLA/Mg-

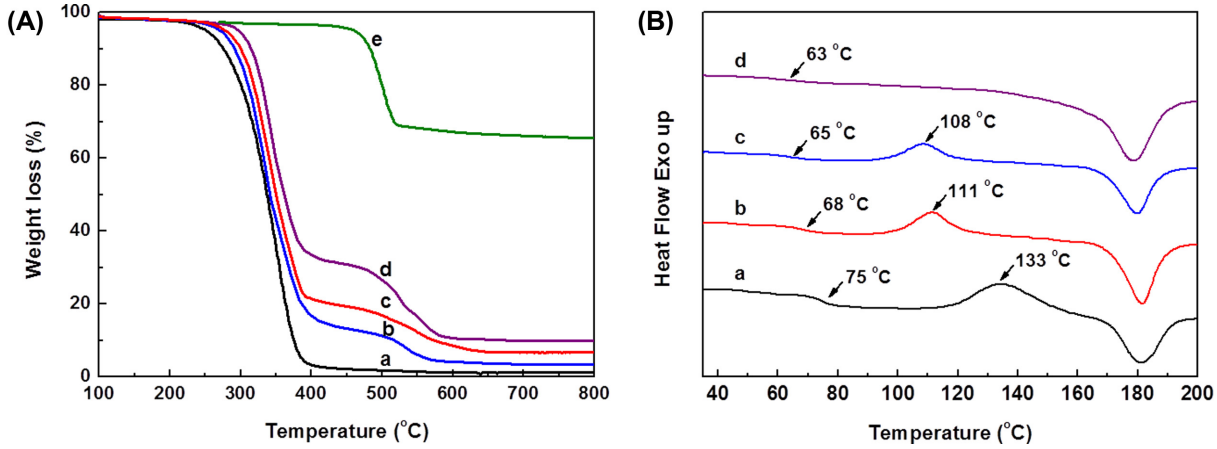

Figure 3. (A) TGA thermograms and (B) DSC traces of (a) PLLA only, (b) PLLA/Mg-Rod150 10%, (c) PLLA/Mg-Rod150 20%, (d) PLLA/Mg-Rod150 30% composites, and (e) Mg-Rod150.

Table II. T_g and T_c of PLLA/Mg(OH)$_2$ Crystalline

Sample	10%		20%		30%	
	T_g (°C)	T_c (°C)	T_g (°C)	T_c (°C)	T_g (°C)	T_c (°C)
PLLA/Mg-PL60	67	107	61	96	62	-
PLLA/Mg-PL300	65	105	59	-	58	-
PLLA/Mg-Rod150	68	108	65	101	63	-
PLLA/Mg-Rod350	68	107	62	98	62	-

Rod150 0%-30% composites. While the melting temperature (T_m) of PLLA is around 180 °C, those of PLLA/Mg-Rod150 10%, PLLA/Mg-Rod150 20%, and PLLA/Mg-Rod150 30% composites are 68, 65, and 63 °C, respectively. As the Mg-Rod150 content increased in the PLLA film, the glass transition temperature (T_g) decreased. When Mg-Rod150 was added to the PLLA, the free volume of the PLLA chain increased, thus increasing the chain mobility of the polymer and decreasing T_g. In addition, PLLA exhibited a crystallization temperature (T_c) of 133 °C, and as the content of Mg-Rod150 (10%-30%) increased, T_c decreased from 111 to 108 °C. The broad T_c peak of pure PLLA appeared due to the slow speed of crystallization. The T_c of the PLLA/Mg-Rod150 composites decreased as the crystallization speed of PLLA was accelerated with increasing Mg-Rod150 content. The sharp T_c peaks of PLLA/Mg-Rod150 composites also appeared.

The T_g and T_c of Mg-Rod350, Mg-PL60, and Mg-PL300 are listed in Table II. The T_g of the PLLA/Mg-Rod350 30% and PLLA/Mg-PL300 30% composites were 58 and 56 °C, respectively, which were lower than the 63 °C of the PLLA/Mg-Rod150 30% and the 62 °C of the PLLA/Mg-PL60 30% composite. Therefore, it is suggested that the Mg-PLs have a stronger effect on the movement of the PLLA chain than the Mg-Rods because of the irregular shape of the Mg(OH)$_2$ plate.

Figure 4 shows the mechanical properties of PLLA/Mg-Rod150, PLLA/Mg-Rod350, PLLA/Mg-PL60, and PLLA/Mg-PL300 (0%-30%) composites. The tensile strength of PLLA was determined to be 32.7 MPa, and it decreased to 29.8 and 17.6 MPa as the content of Mg-Rod150 and Mg-Rod350 increased from 0% to 30%, respectively. Furthermore, the tensile strength decreased to 16.2 and 12.6 MPa as the content of Mg-PL60 and Mg-PL300 increased from 0% to 30% (Figure 4(A)). The elongation at break of PLLA/Mg-Rod150 and PLLA/Mg-Rod350 was reduced from 116.4 to 61.2 and 52.9%, respectively, as the weight percentage of Mg-Rod150 and Mg-Rod350 increased from 0% to 30%, respectively. The elongation of PLLA/Mg-PL60 and PLLA/Mg-PL300 composites also decreased to 21.9% and 16.7%, respectively (Figure 4(b)). In addition, the modulus of PLLA was observed to be 602 MPa and the moduli of PLLA/Mg-Rod150 and PLLA/Mg-Rod350 increased to 1,145 and 948 MPa, respectively with the increase in the content of Mg-Rod150 and Mg-Rod350 from 0

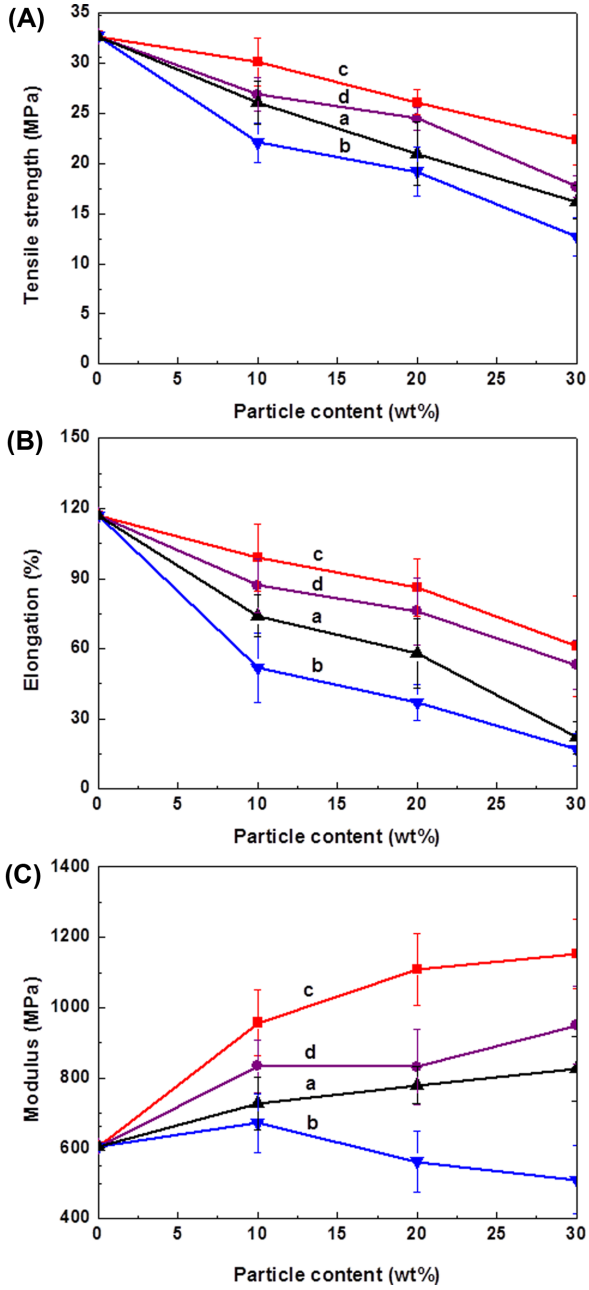

Figure 4. (A) Tensile strength, (B) elongation, and (C) modulus of (a) PLLA/Mg-PL60, (b) PLLA/Mg-PL300, (c) PLLA/Mg-Rod150, and (d) PLLA/Mg-Rod350 composites.

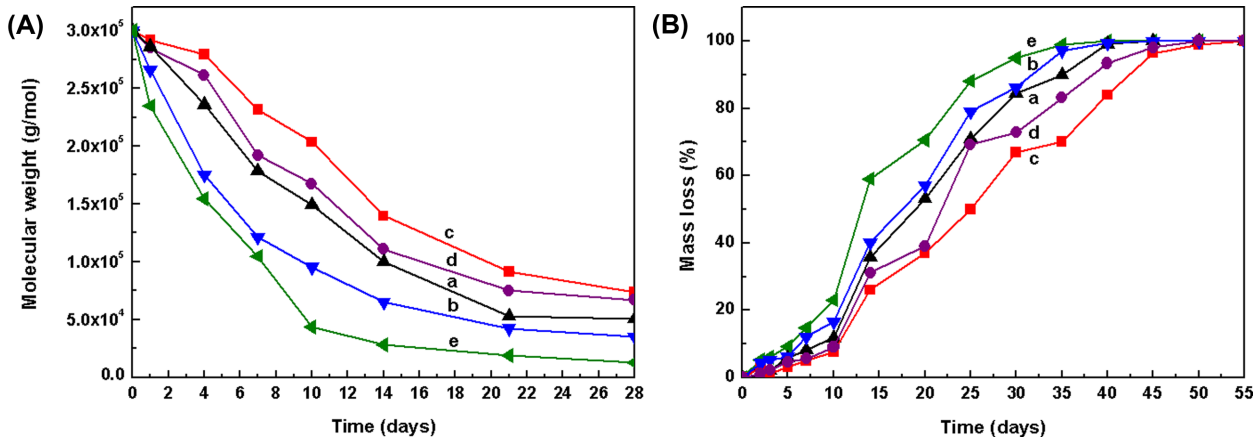

Figure 5. The changes in (A) molecular weight (0-28 days) and (B) mass loss (0-55 days) of (a) PLLA/Mg-PL60 30%, (b) PLLA/Mg-PL300 30%, (c) PLLA/Mg-Rod150 30%, (d) PLLA/Mg-350 30% composites, and (e) PLLA only.

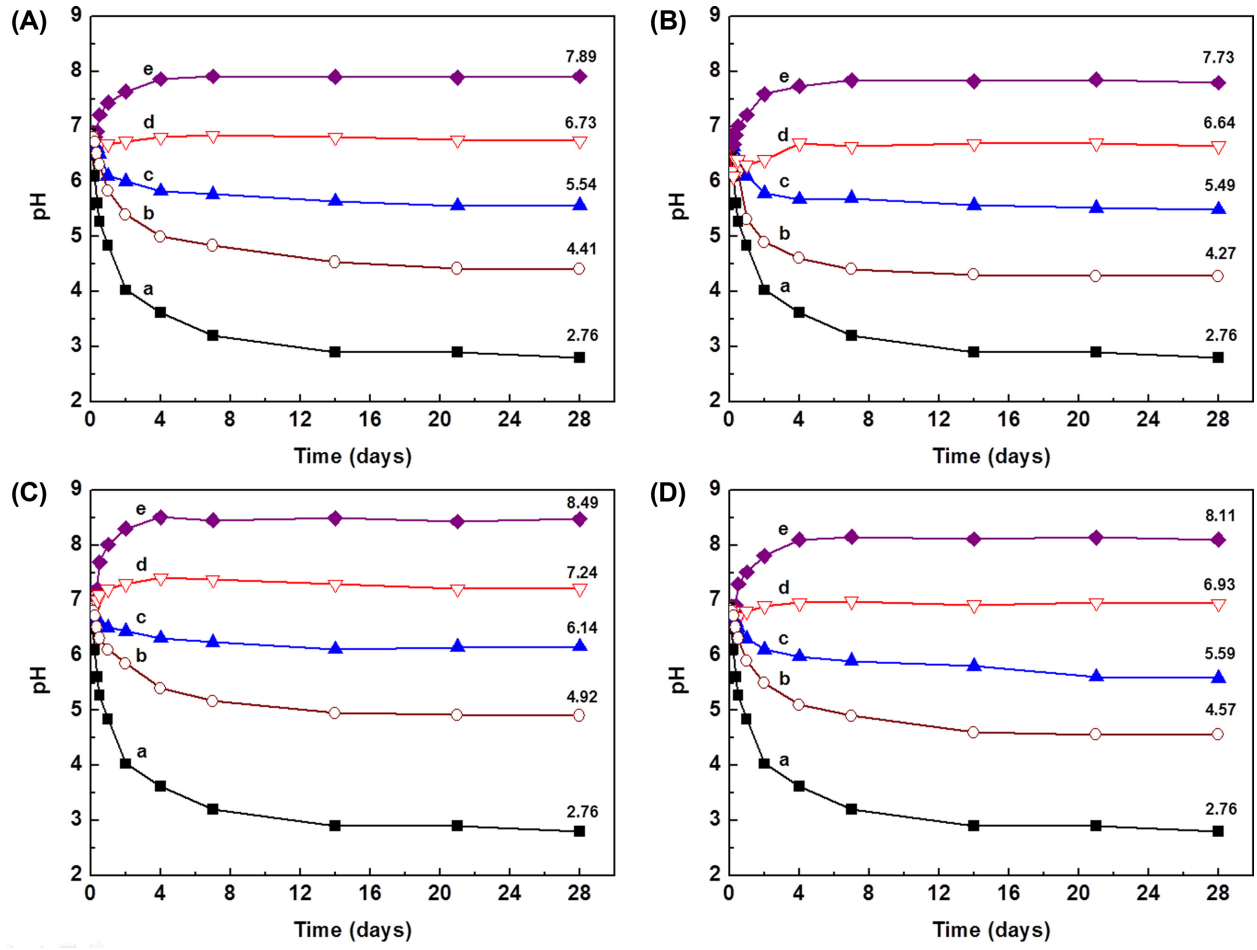

Figure 6. pH changes by the byproduct of (A) PLLA/Mg-PL60, (B) PLLA/Mg-PL300, (C) PLLA/Mg-od150, and (D) PLLA/Mg-Rod350 composites at $Mg(OH)_2$ concentrations of (a) 0, (b) 10, (c) 20, (d) 30, and (e) 40 wt%.

to 30%. The moduli of PLLA/Mg-PL60 and PLLA/Mg-PL300 increased to 825 and 508 MPa, respectively (Figure 4(c)).

The tensile strength and elongation of PLLA/Mg-Rod150, PLLA/Mg-Rod350, PLLA/Mg-PL60, and PLLA/Mg-PL300 30% composites were 10-60% and 50-80%, respectively, lower than those of PLLA because of the poor compatibility of magnesium hydroxide itself with most polymers. The tensile strength of PLLA/Mg-Rod150 was approximately 50%

higher than that of PLLA/Mg-PL300 and the elongation and modulus of PLLA/Mg-Rod150 was about two and four times higher than that of PLLA/Mg-PL300, respectively. Therefore, it seems that the mechanical property of PLLA/Mg-Rods composite was enhanced by advantage of crystalline orientation in PLLA matrix than that of PLLA/Mg-PLs composite.

pH Effect on Byproduct of PLLA/Mg(OH)$_2$ Composites. Figure 5 displays the changes in the molecular weight (M_w) and mass loss of PLLA, PLLA/Mg-Rod150, PLLA/Mg-Rod350, PLLA/Mg-PL60, and PLLA/Mg-PL300 30% composites. The PLLA was degraded by hydrolysis, and it was well-known that the decomposition of PLLA generated the reduction of molecular weight, followed by mass loss.[29] The M_w of the PLLA, PLLA/Mg-Rod150 composite, and PLLA/Mg-Rod350 composite decreased to 1200, 75, and 65 k, respectively, from 300 k in 28 days, whereas those of PLLA/Mg-PL60 and PLLA/Mg-PL300 decreased to 50 and 35 k, respectively. The M_w of the PLLA/Mg(OH)$_2$ composites decreased less than the M_w of PLLA due to the pH neutralization of acidic material by Mg(OH)$_2$. In particular, the M_w of PLLA/Mg-Rod150 and PLLA/Mg-Rod350 were lower than the M_w of PLLA/Mg-PL60 and PLLA/Mg-PL300 (Figure 5(A)). While the PLLA (14 days; 59%) showed the fastest mass loss, the mass loss of PLLA/Mg-Rod150 (25%) and PLLA/Mg-Rod350 (30%) were slower than those of PLLA/Mg-PL60 (36%) and PLLA/Mg-PL300 (41%) (Figure 5(B)). It means that the decrease in Mw and mass loss was much more slowly accomplished in PLLA/Mg-Rod150 composite because the Mg-Rod150 rod has higher solubility as compared to Mg-Rod350, Mg-PL60, and Mg-PL300.

Figure 6 shows the pH changes of PLLA, PLLA/Mg-Rod150, PLLA/Mg-Rod350, PLLA/Mg-PL60, and PLLA/Mg-PL300 (0%-30%) composites for 28 days. The degradation of PLLA was accelerated under a harsh condition (80 ºC and 100 rpm), resulting in the decrease of pH to 2.76 in 28 days. The decreased pH was due to the generation of lactic acid as a degradation byproduct. However, the pH of the PLLA/Mg-Rod150 composite increased from 2.76 to 8.49 as the weight percentage of Mg-Rod150 increased from 0% to 40% for 28 days. The pH of PLLA/Mg-Rod350, PLLA/Mg-PL60, and PLLA/Mg-PL300 (0-30%) composites increased from 2.76 to 8.11, 7.89, and 7.73, respectively. In particular, the PLLA/Mg-150 composite

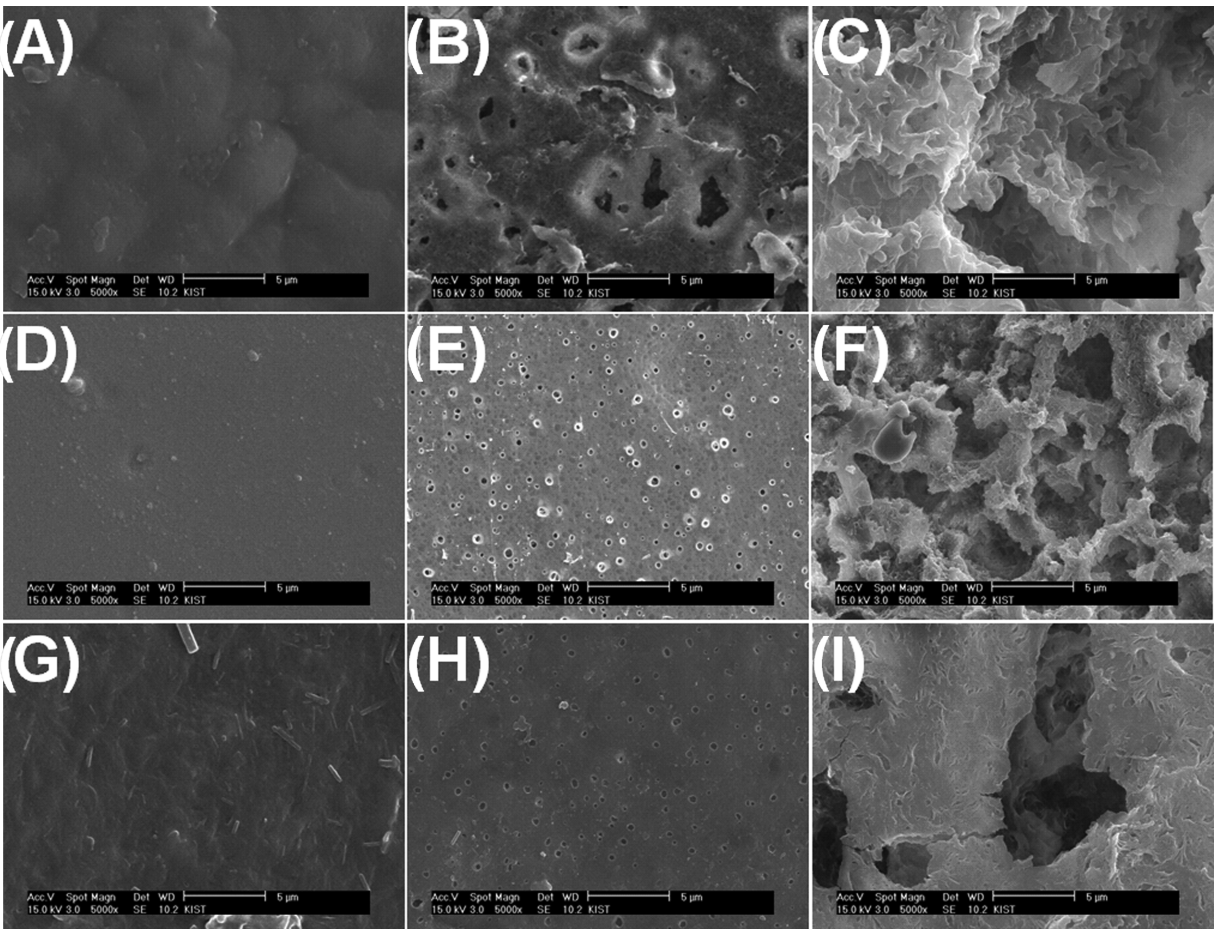

Figure 7. SEM images of the degraded surface of PLLA for (A) 0 day, (B) 7 days, and (C) 14 days, PLLA/Mg-PL60 for (D) 0 day, (E) 7 days, and (F) 14 days, and PLLA/Mg-Rod150 for (G) 0 day, (H) 7 days, and (I) 14 days. The magnification of the images is ×5,000.

was shown to indicate a higher pH than PLLA/Mg-Rod350, PLLA/Mg-PL60, and PLLA/Mg-PL300 composites with the same contents. The pH of PLLA/Mg-Rod150 30% composite was 7.24, whereas those of PLLA/Mg-Rod350, PLLA/Mg-PL60, and Mg-PL300 30% composites was 6.93, 6.73, and 6.63, respectively. Such difference seem to have occurred because of the high solubility of Mg-Rod150 as compared to Mg-Rod300, Mg-PL60, and Mg-PL350, which resulted in a higher pH and the reduction in the film decomposition rate that neutralizes an acidic environment caused by the degradation of its byproducts.

Figure 7 presents the SEM images of the film surfaces of PLLA, PLLA/Mg-PL300, and PLLA/Mg-Rod150 30% composites, showing the decomposition at 0, 7, and 14 days, respectively. The SEM images of PLLA, PLLA/Mg-PL300, and PLLA/Mg-Rod150 were observed to decompose through bulk erosion. The SEM images (7 days) revealed that PLLA/Mg-PL300 and PLLA/Mg-Rod150 formed small pores, in contrast to the PLLA film. In addition, the SEM images of 14 days showed the surface of the PLLA film to be almost completely decomposed, but those of PLLA/Mg-PL300 and PLLA/Mg-Rod150 still retained their original forms to a substantial degree. In particular, the surface of PLLA/Mg-Rod150 decomposed less than that of PLLA/Mg-PL300.

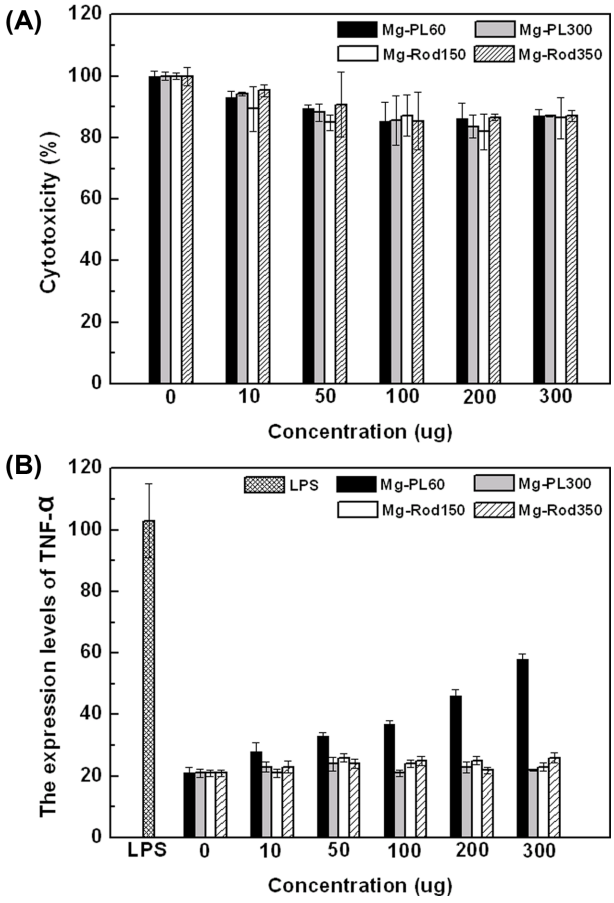

Figure 8. (A) The cytotoxicity and (B) the expression levels of TNF-α of Mg-PL60, Mg-PL300, Mg-Rod150, and Mg-PL300 (1-300 μg) on U937 cell.

Inflammation Response to PLLA/$Mg(OH)_2$ Composites. Figure 8 shows the cytotoxicity and inflammatory response of the Mg-Rod150, Mg-Rod350, Mg-PL60, and Mg-PL300 on U-937 cell. Although the concentration of Mg-Rod150 increased from 1 to 300 mg, the cytotoxicity of Mg-Rod150 did not decrease to less than 80%. The cytotoxicity of Mg-Rod350, Mg-PL60, and Mg-PL300 also displayed a similar tendency as that of Mg-Rod150, meaning high biocompatibility of $Mg(OH)_2$. (Figure 8(A)) In addition, the expression level of TNF-α during U-937 cell culture was determined by ELISA with increasing the concentrations of Mg-Rod150, Mg-Rod350, Mg-PL60, and Mg-PL300. When lipopolysaccharide (LPS, positive control) was used to induce the inflammatory response of U-937 cells, the expression levels of TNF-α increased considerably as compared to the normal condition at LPS concentration of 1.0 μg. This indicates that inflammation was definitely caused by LPS. The expression levels of TNF-α could be detected with 1-300 μg concentration of Mg-Rod150. Furthermore, the expression levels of TNF-α from Mg-Rod350 and Mg-PL300 were also not confirmed. However, the expression levels of TNF-α gradually increased with increasing Mg-PL60 concentrations from 1 to 300 μg. When the size of the particles was below 100 nm, endocytosis was generated in the cell. This endocytosis is known to cause potential cytotoxicity due to the inflammation response of the cell.[30-32] Therefore, potential cytotoxicity possibly appeared in Mg-PL60 (Figure 8(B)).

Figure 9(A) and (B) show the viability of U-937 cells to byproducts of PLLA/Mg-Rod150 and PLLA/Mg-PL300 composites. The degradation of PLLA induced cell death in about 80% of the cells by creating an acidic environment (pH 2.76). However, the byproducts of PLLA/Mg-Rod150 and PLLA/Mg-PL300 showed a lower cytotoxicity when the contents of Mg-Rod150 and Mg-PL300 increased from 0% to 40%. When the concentration of Mg-Rod150 and Mg-PL300 was 20%, PLLA/Mg-Rod150 and PLLA/Mg-PL300 showed a cell viability of above 80%. The cell viability of PLLA/Mg-Rod150 and PLLA/Mg-PL300 composites was similarly appeared. However, when these composites were used within a concentration range of 10%-20%, the cell viability of PLLA/Mg-Rod150 was 10%-20% greater than that observed using PLLA/Mg-PL300. This was due to the higher pH of PLLA/Mg-Rod150 than that of PLLA/Mg-PL300. Figure 9(C) and (D) show the cell viability in the presence of byproducts of PLLA/Mg-Rod150 and PLLA/Mg-PL300 (0%-30%) composites. These results were similar to that of the CCK-8 assay. Figure 9(E) and (F) confirm the expression levels of TNF-α in U-937 cells as inflammatory markers in the presence of byproducts of the PLLA/Mg-Rod150 and PLLA/Mg-PL300 composites. The expression level of TNF-α was determined using the U-937 cell culture medium, which

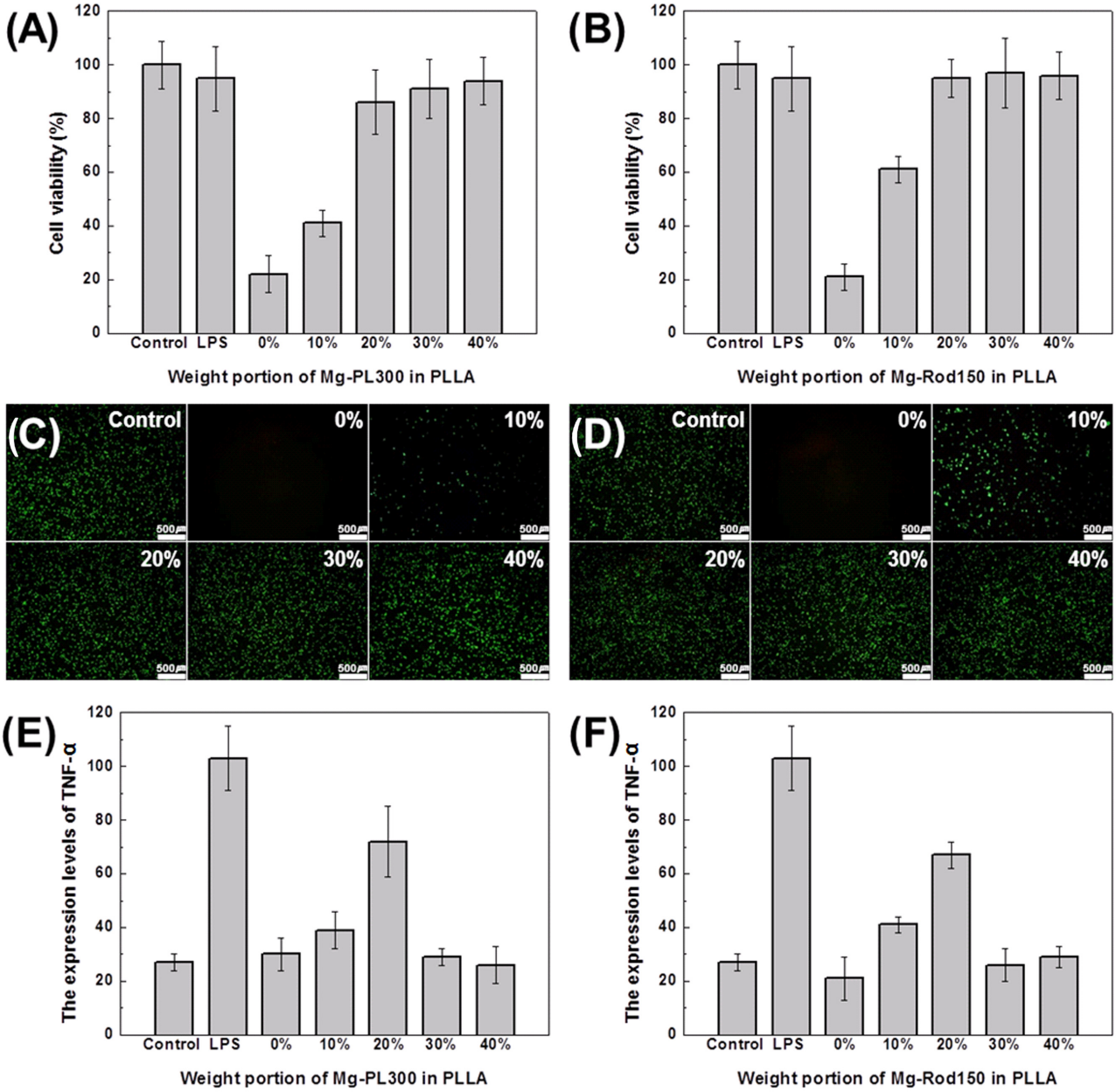

Figure 9. U-937 viability of (A) PLLA/Mg-PL300 and (B) PLLA/Mg-Rod150 composites (0-40 wt%), fluorescence microscopic images of (C) PLLA/Mg-PL300 and (D) PLLA/Mg-Rod150 composites (0-40 wt%), and the expression levels of TNF-α in U-937 culture after the addition of byproducts from (E) PLLA/Mg-PL300 and (F) PLLA/Mg-Rod150 composites (0-40 wt%).

contained effluents from the PLLA matrices that were embedded with different amounts of PLLA/Mg-Rod150 and PLLA/Mg-PL300 composites. The expression level of TNF-α decreased when 0-10 wt% of Mg-Rod150 and Mg-PL300 were used in the PLLA matrix. TNF-α was highly expressed at 10 wt% Mg-Rod150 and Mg-PL300. The expression level of TNF-α gradually decreased for Mg-Rod150 and Mg-PL300, from 10 to 40 wt%. This result suggests that the expression level of TNF-α was reduced by pH neutralization. The expression level of TNF-α in the PLLA/Mg-Rod150 composite exhibited a similar pattern to that for the PLLA/Mg-PL300.

Consequently, although the cytotoxicity of $Mg(OH)_2$ rods showed similar results to $Mg(OH)_2$ plates, potential cytotoxicity was discovered *via* the expression level of TNF-α in Mg-PL60. In addition, the byproduct of PLLA/Mg-Rods composite was more effectively neutralized than that of the PLLA/Mg-PLs composite, but cell viability and the expression levels of TNF-α was similarly appeared.

Conclusions

Mg-Rods and Mg-PLs were successfully synthesized *via* hydrothermal and base precipitation methods, and were blended with a PLLA. Although the tensile strength and elongation of PLLA/Mg-Rods and PLLA/Mg-PLs decreased owing to poor compatibility between $Mg(OH)_2$ and PLLA, PLLA/Mg-Rods exhibited higher values than PLLA/Mg-PLs. In particular, the modulus of PLLA/Mg-Rod150 30% composite was 50% improved as compared to PLLA/Mg-PL300. PLLA/Mg-Rod150 showed more mass loss and molecular weight loss, as compared to PLLA/Mg-Rod350, PLLA/Mg-PL60, and PLLA/Mg-PL300 by high pH environment of PLLA/Mg-Rod150. In addition, the cyototoxicity of Mg-Rods and Mg-PL was not discovered but potential cytotoxicity of Mg-PL60 was generated by endocytosis. U-937 cell viability of PLLA/Mg-Rod150 and PLLA/Mg-PL300 composites was observed to increase as the content of Mg-Rod150 and Mg-PL300 increased from 0 to 40% and the level of TNF-a expression decreased with increasing Mg-Rod150 and Mg-PL300 content. In particular, PLLA/Mg-Rod150 (pH 7.24) had positive effect in cell viability by higher pH environment than PLLA/Mg-PL300 (pH 6.64).

Therefore, the PLLA/Mg-Rods composite system showed more advantages over PLLA/Mg-PLs in mechanical properties and pH neutralization of an acidic environment, and the possible enhancement in the inflammatory response and mechanical properties of the biodegradable polymers was confirmed for biomedical implants.

Acknowledgments. This work was supported by Cell Regeneration Program (2012M3A9C6049717) and National Research Foundation (NRF) (2013034945, 2013009045) funded by the Ministry of Science, ICT & Future Planning (MSIP), and Core Materials Technology Development Program (10048019) and Advanced Medical New Material(Fiber) Development Program (A006100055) funded by the Ministry of Trade, Industry and Energy (MOTIE), Korea.

References

(1) B. Jeong, Y. H. Bae, D. S. Lee, and S. W. Kim, *Nature*, **388**, 860 (1997).
(2) L. E. Freed, G. Vunjak-Novakovic, R. J. Biron, D. B. Eagles, D. C. Lesnoy, S. K. Barlow, and R. Langer, *Nat. Biotechnol.*, **12**, 689 (1994).
(3) Y. K. Joung, B. N. Jang, J. H. Kang, and D. K. Han, *Biomater. Biomed. Eng.*, **1**, 13 (2014).
(4) C. H. Park, Y. J. Hong, K. Park, and D. K. Han, *Macromol. Res.,* **18**, 526 (2010).
(5) G. Khang, J. M. Rhee, P. Shin, I. Y. Kim, B. Lee, S. J. Lee, Y. M. Lee, H. B. Lee, and I. Lee, *Macromol. Res.,* **10**, 158 (2002).
(6) M. Dunne, O. I. Corrigan, and Z. Ramtoola, *Biomaterials*, **21**, 1659 (2000).
(7) K. H. Lam, J. M. Schakenraad, H. Groen, H. Esselbrugge, P. J. Dijkstra, J. Feijen, and P. Nieuwenhuis, *J. Biomed. Mater. Res.,* **29**, 929 (1995).
(8) W. J. van der Giessen, A. M. Lincoff, R. S. Schwartz, H. M. M. van Beusekom, P. W. Serruys, D. R. Holmes, S. G. Ellis, and E. J. Topol, *Circulation*, **94**, 1690 (1996).
(9) T. Inoue, K. Croce, T. Morooka, M. Sakuma, K. Node, and D. I. Simon, *J. Am. Coll. Cardiol.*, **4**, 1057 (2011).
(10) J. M. Anderson, A. Rodriguez, and D. T. Chang, *Semin Immunol.*, **20**, 86 (2008).
(11) R. Kontio, P. Ruuttila, L. Lindroos, R. Suuronen, A. Salo, C. Lindqvist, I. Virtanen, and Y. T. Konttinen, *Int. J. Oral Maxillofac. Surg.,* **34**, 766 (2005).
(12) F. Vogt, A. Stein, G. Rettemeier, N. Krott, R. Hoffmann, J. vom Dahl, A.-K. Bosserhoff, W. Michaeli, P. Hanrath, C. Weber, and R. Blindt, *Eur. Heart J.,* **25**, 1330 (2004).
(13) O. Petillo, G. Peluso, L. Ambrosio, L. Nicolais, W. J. Kao, and J. M. Anderson, *J. Biomed. Mater. Res.,* **28**, 635 (1994).
(14) C. T. Hanks, J. C. Wataha, and Z. Sun, *Dent. Mater.*, **12**, 186 (1996).
(15) C. H. Kum, Y. J. Cho, Y. K. Joung, J. Y. Choi, K. D. Park, S. H. Seo, Y. S. Park, D. J. Ahn, and D. K. Han, *J. Mater. Chem. B*, **1**, 2764 (2013).
(16) S.-Y. Fu, X.-Q. Feng, B. Lauke, and Y.-W. Mai, *Compos. Part B: Eng.,* **39**, 933 (2008).
(17) B. Y. Shin, G. S. Jo, K. S. Kang, T. J. Lee, B. S. Kim, S. I. Lee, and J. S. Song, *Macromol. Res.,* **15**, 291 (2007).
(18) D. Chen, L. Zhu, P. Liu, H. Zhang, K. Xu, and M. Chen, *J. Porous Mater.,* **16**, 13 (2009).
(19) C. Henrist, J.-P. Mathieu, C. Vogels, A. Rulmont, and R. Cloots, *J. Cryst. Growth,* **249**, 321 (2003).
(20) Y. Li, M. Sui, Y. Ding, G. Zhang, J. Zhuang, and C. Wang, *Adv. Mater.,* **12**, 818 (2000).
(21) J. Lv, L. Qiu, and B. Qu, *Nanotechnology*, **15**, 1576 (2004).
(22) M. Hayashi, H. Muramatsu, M. Sato, Y. Tomizuka, M. Inoue, and S. Yoshimoto, *J. Craniomaxillofac. Surg.,* **41**, 783 (2013).
(23) W. Jiang, B. Y. S. Kim, J. T. Rutka, and W. C. W. Chan, *Nat. Nanotechnol.,* **3**, 145 (2008).
(24) D. Chen, L. Zhu, P. Liu, H. Zhang, K. Xu, and M. Chen, *J. Porous Mater.,* **16**, 13 (2009).
(25) Y. Xiong, B. Wua, J. Zhu, X. Fan, P. Cai, J. Wen, and X. Liu, *Hydrometallurgy,* **142**, 137 (2014).
(26) Y. Ding, G. Zhang, H. Wu, B. Hai, L. Wang, and Y. Qian, *Chem. Mater.,* **13**, 435 (2001).
(27) H. W. Lee, S. H. Seo, C. H. Kum, B. J. Park, Y. K. Joung, T. I. Son, and D. K. Han, *Macromol. Res.,* **22**, 210 (2014).
(28) Y. Li and X. S. Sun, *Biomacromolecules*, **11**, 1847 (2010).
(29) I. C. McNeill and H. A. Leiper, *Polym. Degrad. Stab.*, **11**, 309 (1985).
(30) S. Xiong, S. George, H. Yu, R. Damoiseaux, B. France, K. Woei Ng, and J. S.-C. Loo, *Arch. Toxicol.,* **87**, 1075 (2013).
(31) M. V. D. Z. Park, A. M. Neigh, J. P. Vermeulen, L. J. J. de la Fonteyne, H. W. Verharen, J. J. Briedé, H. van Loveren, and W. H. de Jong, *Biomaterials,* **32**, 9810 (2011).
(32) F. Zhao, Y. Zhao, Y. Liu, X. Chang, C. Chen, and Y. Zhao, *Small,* **1**, 1322 (2011).